Published in final edited form as:
Nat Biotechnol. ; 30(2): 165–173. doi:10.1038/nbt.2107.

Generation of human vascular smooth muscle subtypes provides insight into embryological origin-dependent disease susceptibility

Christine Cheung[1,2], **Andreia S Bernardo**[1], **Matthew W B Trotter**[1], **Roger A Pedersen**[1], and **Sanjay Sinha**[1,2]

[1]The Anne McLaren Laboratory for Regenerative Medicine, University of Cambridge, West Forvie Building, Forvie Site, Robinson Way, Cambridge CB2 0SZ, United Kingdom.

[2]Division of Cardiovascular Medicine, University of Cambridge, ACCI Level 6, Box 110, Addenbrooke's Hospital, Hills Road, Cambridge CB2 0QQ.

Abstract

Heterogeneity of embryological origins is a hallmark of vascular smooth muscle cells (SMCs), which may influence vascular disease development. Differentiation of human pluripotent stem cells (hPSCs) into developmental origin-specific SMC subtypes remains elusive. In this study, we have established a chemically defined protocol where hPSCs were initially induced to form neuroectoderm, lateral plate mesoderm or paraxial mesoderm. These intermediate populations were further differentiated towards SMCs (>80% $MYH11^+$ and $ACTA2^+$) which displayed contractile ability in response to vasoconstrictors and invested perivascular regions *in vivo*. Derived SMC subtypes recapitulated the unique proliferative and secretory responses to cytokines previously documented in studies using aortic SMCs of distinct origins. Importantly, this system predicted increased extracellular matrix degradation by SMCs derived from lateral plate mesoderm, which was confirmed using rat aortic SMCs from corresponding origins. Collectively, this work will have broad applications in modeling origin-dependent disease susceptibility and in bio-engineered vascular grafts for regenerative medicine.

Introduction

Vascular SMCs and pericytes comprise the walls of larger vessels and capillary beds respectively[1]. Interestingly, lineage tracking studies have shown that vascular SMCs in different vessels have distinct embryological origins[2]. For example, the basal aortic root is derived from secondary heart field[3] while the ascending aorta and the arch are neural crest derived[4]. Descending aortic SMCs originate from paraxial/somitic mesoderm[5]. Coronary SMCs arise from the pro-epicardial organ which is of lateral plate mesodermal origin[6]. Although information on the embryological origins of pericytes is relatively lacking, there is considerable phenotypic overlap between these cells and SMCs. Consistent with the

Correspondence should be addressed to S.S. (ss661@cam.ac.uk)..

Author contributions: C.C. and S.S. developed the concept of generating origin-specific SMCs and designed the experiments. A.S.B. and R.A.P. developed the mesoderm specification protocols. C.C. performed experiments, analyzed data, wrote and prepared the manuscript. A.S.B. performed part of the mesoderm validation experiments. M.W.B.T. advised regarding design of the microarray experiment, processed the resulting data, and contributed to further analysis. S.S. supervised the project. All co-authors edited the manuscript.

Competing financial interests: The authors declare no competing financial interests.

Europe PMC Funders Author Manuscripts

phenotypic similarities, it appears that SMCs and pericytes in the same vascular region share common origins[7-10].

The diversity of SMC origins may in part contribute to the site-specific localization of vascular diseases including regional susceptibility to atherosclerosis[11, 12], vascular calcification[13] and aortic aneurysm distribution[14]. Notably, aortic dissections occur preferentially at the interfaces where SMCs of distinct embryological origins meet. Together these findings suggest that intrinsic lineage-derived differences between SMCs may play a role in the spatiotemporal pattern of vascular diseases. Therefore, a model system to investigate how SMC embryological origins influence development of vascular diseases would be valuable.

Currently, SMC derivation from human embryonic or induced pluripotent stem cells (hESCs or iPSCs), collectively known as hPSCs usually requires serum and does not encompass the concept of using a lineage-specific approach[15]. We report a chemically defined method for generating origin-specific SMCs from hPSCs via three intermediate lineages – neuroectoderm, lateral plate mesoderm and paraxial mesoderm. We used our *in vitro* system to predict the responses of different SMC subtypes to interleukin-1β (IL-1β), an inflammatory mediator, and validated the results using rat aortic SMCs of distinct origins. Our finding reveals that origin-specific SMCs exhibit differential activation of matrix metalloproteinase 9 (MMP9) and tissue inhibitor of metalloproteinase 1 (TIMP1). Hence, our SMC subtypes could potentially be used to study origin-dependent disease susceptibility and also serve as a source of therapeutic cells for vascular regenerative medicine.

Results

Mesoderm subtypes can be specified by manipulation of BMP and PI3K pathways

The H9 hESC line, which is chromosomally normal (Supplementary Fig. 1a), was used to study the specification of the various lineages from which SMCs arise. For neuroectoderm differentiation, we adopted our previously published protocol[16], using fibroblast growth factor 2, (FGF2, 12 ng/ml) and the activin/nodal inhibitor, SB431542 (10 μM). During the induction of neuroectoderm in hESCs, we observed a marked decrease in expression of the pluripotency marker, *NANOG*, within 2 days (Supplementary Fig. 1b). The expression of neuroectoderm markers (*GBX2*, *OLIG3* and *SOX1*) increased over time and peaked between day 6 and day 8, as documented before[16]. Extensive immunostaining for neuroectoderm markers (PAX6 and NESTIN) was observed in both hESCs and human iPSCs after 7 days of FGF2 and SB431542 treatment. High efficiency of neuroectoderm induction was observed with over 90% of the cells double positive for PAX6 and NESTIN (Supplementary Fig. 1c). For mesoderm subtype differentiation, we utilized our previously described 36-hour early mesoderm differentiation protocol[17]. A combination of FGF2 (20 ng/ml), phosphoinositide 3-kinase (PI3K) inhibitor (LY294002, 10 μM) and b**one morphogenetic protein** 4 (BMP4, 10 ng/ml), herein referred to as FLyB, was used (Fig. 1ai). Subsequent mesoderm subtype specification was further investigated.

During embryogenesis, specification of lateral plate mesoderm and paraxial mesoderm follows a posterior-anterior BMP gradient along the primitive streak[18] (Fig 1aii). We hypothesized that by varying the BMP4 concentration according to these developmental principles, we would obtain the relevant mesoderm subtypes from hPSCs. Studies have suggested that BMP signaling is a key driver of mesoderm[19-22] and BMP4 also cooperates with ActivinA to induce differentiation of mesendoderm, the precursor of mesoderm and endoderm[16]. We examined the roles of BMP4 and ActivinA in mesoderm subtype specification from the early mesoderm stage while keeping FGF2 (20 ng/ml) and LY294002 (10 μM) constant. In the presence of ActivinA (10 ng/ml, black bars), BMP4 promoted the

expression of the lateral plate marker, *KDR*, in a dose-dependent way (from 0 ng/ml to 100 ng/ml, i.e. B0 to B100, respectively) (Fig. 1b). Endogenous BMP signaling (B0 condition) was insufficient to promote *KDR* expression since Noggin (Nog), a BMP antagonist, produced the same effect as B0. Absence of ActivinA (white bars) did not affect the development of lateral plate mesoderm since *KDR* was expressed as long as BMP4 was added. In contrast, absence of ActivinA promoted the expression of the paraxial marker, *MEOX1*, in the absence of BMP (Nog and B0 conditions). ActivinA was therefore dispensable for mesoderm formation while high concentration of BMP4 enhanced lateral plate mesoderm specification but inhibited paraxial mesoderm specification.

We then evaluated the effect of LY294002 (Ly, 10 μM) on mesoderm subtype specification. Ly has been shown to facilitate differentiation of hESCs[23]. Interestingly we found that, in the presence of FGF2 (F, 20 ng/ml) alone, Ly (10 μM, black bars) significantly promoted the expression of a panel of paraxial markers, *MEOX1* ($P = 0.0051$), *TBX6* ($P = 0.0027$), *TCF15* ($P = 0.0001$) and *PAX1* ($P = 0.0087$), versus no Ly (white bars) (Fig. 1c). Again, the presence of BMP4 (B50, 50 ng/ml) inhibited the expression of all paraxial markers and promoted the expression of lateral plate markers. On the other hand, Ly significantly downregulated the lateral plate markers, *LMO2* ($P = 0.00024$ in F, $P = 0.00002$ in FB50), *PECAM1* ($P = 0.0037$ in F, $P = 0.00167$ in FB50), *NKX2-5* ($P = 0.0170$ in F) and *ISL1* ($P = 0.0132$ in F) compared to the no Ly condition. Hence, we established the optimal conditions for lateral plate and paraxial mesoderm sub-specification to be FB50 (FGF2, 20 ng/ml + BMP4, 50 ng.ml) and FLy (FGF2, 20 ng/ml + LY294002, 10 μM) respectively.

We next determined the time-scale of mesoderm subtype differentiation. *NANOG* expression decreased markedly within 2 days of differentiation of hESCs (Fig. 1d). Brachyury (*T*), a primitive streak and early mesoderm marker, emerged transiently and peaked at 36 hours after FLyB treatment. Further specification demonstrated that FB50 (red lines) increased the expression of lateral plate genes (*MESP1*, *KDR*, *NKX2-5* and *ISL1*) from as early as day 2 of differentiation and, peaking at days 4 to 5. In contrast, FLy (blue lines) upregulated paraxial genes (*TBX6*, *MEOX1*, *TCF15* and *PAX1*) only, with peak expression between days 3 and 5. Flow cytometry confirmed that FB50 (white bars) treatment significantly promoted lateral plate mesoderm development, with 82.4 ± 5.1% KDR-expressing cells at day 5 compared to 2.12 ± 0.21% under the FLy (black bars) treatment ($P = 0.0004$) (Supplementary Fig. 1d). Meanwhile, FLy treatment resulted in 67.5 ± 7.3% TCF15-expressing cells at day 5, versus 1.25 ± 0.05% using FB50 ($P = 0.0008$), indicative of paraxial mesoderm formation primarily. Representative flow cytometric plots are shown in Fig. 1e. Day 5 populations generated by either FB50 or FLy treatment also stained positively for their respective mesoderm subtype markers by immunofluorescence (Fig. 1f). We therefore identified day 5 as the time point when the relevant mesoderm subtypes were optimally specified (Fig. 1d-f, Supplementary Fig. 1c). In summary, we devised for the first time, a method to derive either paraxial or lateral plate mesoderm subtypes from hESCs.

Vascular SMC subtypes are generated with high efficiency from three intermediate lineages

During vessel development, platelet-derived growth factor BB (PDGF-BB) induces differentiation of mesenchymal progenitors into vascular SMCs[24]. Upon investment of SMCs to the newly formed blood vessels, transforming growth factor-beta 1 (TGF-β1) promotes SMC maturation and regulates vessel remodeling[24]. We tested the effects of PDGF-BB (10 ng/ml) and TGF-β1 (2 ng/ml), as well as two other SMC inducers, retinoic acid (RA, 1 μM) and sphingosylphosphorylcholine (SPC, 5 μM), on our derived intermediate populations, namely neuroectoderm (NE), lateral plate mesoderm (LM) and paraxial mesoderm (PM). A combination of the two best inducers, PDGF-BB and TGF-β1

[PT treatment (PDGF-BB, 10ng/ml + TGF-β1, 2ng/ml)], promoted the highest expression of the SMC marker, *MYH11*, from all the intermediate populations (Supplementary Fig. 2a). Combined protocols to derive origin-specific SMCs from hPSCs are outlined in Fig. 2a. Henceforth, we will refer to the neuroectoderm-derived SMC, lateral plate mesoderm-derived SMC and paraxial mesoderm–derived SMC as NE-SMC, LM-SMC and PM-SMC respectively (Fig. 2a).

The expression of multiple SMC markers increased over time with PT treatment and peaked between day 9 and day 12 with upregulation of early SMC markers (*ACTA2*, *TAGLN*, *CNN1*) preceding the late markers (*SMTN*, *MYH11*) (Fig. 2b). The derived SMCs after 12 days of PT treatment demonstrated comparable gene expression levels to the positive control, human aortic SMCs (ASMC) (Supplementary Fig. 2b). Flow cytometric analysis correlated with the gene expression data documenting an increment in the percentage of cells doubly positive for MYH11 and ACTA2 over this period (Supplementary Fig. 2c). Twelve days of PT treatment culminated in over 80% $MYH11^+/ACTA2^+$ cells generated from the three intermediate populations, comparable to ASMC. A small proportion of cells in the intermediate populations (3-8%) and during early SMC differentiation (2-7%) expressed the pericyte marker, CSPG4 (Supplementary Fig. 2d). Notably, there was little or no co-expression of CSPG4 and MYH11 suggesting that differentiating cells could adopt either a SMC or a pericyte-like phenotype. By day 12 of PT treatment, the pericyte-like population diminished, suggesting that the differentiation conditions had selected for SMCs (>86% $MYH11^+$). Two isoforms of smoothelin, namely smoothelin-A and smoothelin-B, have been reported to be specifically expressed in the visceral and vascular SMCs respectively[25]. Our derived SMCs exhibited up to ten fold lower smoothelin-A expression levels than human gut derived sample although smoothelin-B expression was comparable to ASMC, suggesting that the differentiation conditions favored vascular SMC specification (Supplementary Fig. 2e). This highly efficient process to derive origin-specific SMCs was reproducible in two hESC lines (H1 and H9), and a wild-type iPSC line (Fig. 2c).

Since vascular SMCs arise more precisely from the neural crest, a descendant of neuroectoderm, we investigated whether there was transient formation of neural crest during neuroectoderm to SMC differentiation. Indeed, expression of *BMP4* and *BMP7*, required for neural crest differentiation[26], increased following PT treatment, prior to the peak expression of neural crest markers, *SNAI1* and *SNAI2* at day 3 (Supplementary Fig. 2f). The other neural crest markers, *PAX3* and *SOX10*, displayed higher expression during the first 2 days of PT treatment as *BMP* expression levels increased. We reasoned that the spontaneous formation of neural crest could be due to the endogenous production of BMP4 and BMP7.

Microarray analysis was performed to characterize the hPSC-derived SMCs. Differentiated SMCs demonstrated a downregulation of pluripotency genes, accompanied by upregulation of vascular SMC genes (Fig. 2d). Furthermore, genes relating to neuronal, cardiac/endothelial/hematopoietic and skeletal muscle lineages, which are the other potential derivatives of neuroectoderm, lateral plate mesoderm and paraxial mesoderm respectively, were repressed. Immunocytochemistry showed extensive staining for SMC markers in the derived SMCs and positive control, human ASMCs, but not in the negative control, human umbilical vein endothelial cells (HUVECs) (Fig. 2e). Western blot also demonstrated the presence of mature SMC proteins, MYH11 and SMTN, in our derived SMCs and ASMCs, which were absent in HUVECs (Fig. 2f). Overall, these results suggest that by mimicking embryonic development, we developed a robust process to directly differentiate hPSCs into origin-specific SMCs using a series of growth factor manipulations in a chemically defined medium.

Origin-specific vascular SMCs are functional

Despite the divergent initial differentiation routes, microarray analysis revealed that the three types of derived SMCs shared many genes (3,604) differentially upregulated compared to hESC (FDR 0.1%) (Fig. 3a). Among the highly enriched functional classifications of the 3,604 genes, there were the classical SMC functionality categories such as blood vessel morphogenesis, extracellular matrix (ECM) interaction and actin cytoskeleton organization (see Fig. 3a, gene lists of highlighted groups found in Supplementary Table 1). Alternatively, the significantly enriched functional classifications of the non-overlapping gene subsets revealed inherent differences among SMC subtypes (Supplementary Fig. 3a). For example in NE-SMC, there were categories related to myelination and synaptic transmission, both of which are neuronal characteristics, supporting the common neuroectoderm origin of NE-SMC and neurons. In particular, LM-SMC was highly enriched in genes promoting cell migration and consistent with this enrichment, these cells also displayed the greatest migration in a scratch assay (Supplementary Fig. 3b).

To assess SMC contractile potential, we initially performed immunostaining for vinculin and phalloidin staining for actin filaments. Well developed focal adhesion complexes were detected in all three SMC sub-types (Supplementary Fig. 3c). The cells were then preloaded with a calcium-sensitive dye, Fluo-4. Carbachol (100 μM) stimulated an increase in Fluo-4 fluorescence intensity in the derived SMCs within 1 minute of treatment (red, blue and green lines, Fig. 3bi), indicating increased intracellular calcium flux. After 2 minutes of treatment, Fluo-4 intensity decreased, approaching original basal levels by 5 minutes. The same trend was observed in the positive control, human ASMCs (purple line) but not in the negative control HeLa cells (grey line). Freshly dissociated rat aortic SMCs (orange line) served as the optimal physiological control and demonstrated prolonged increase in intracellular calcium over the first 3 minutes. The derived SMCs exhibited comparable peak fluorescence responses to both the cultured and freshly dissociated SMC controls (Fig. 3bii). Time-lapse microscopy showed that our SMCs and ASMCs contracted in a tonic fashion during the 10 minutes of carbachol treatment (Fig. 3c and Supplementary Videos 1-5), consistent with the sustained contraction usually manifested by vascular SMCs in controlling vessel tone. Contracting cells exhibited between 10-20% change of cell surface area ($n = 20$). Over 50% and 20% of all derived SMCs contracted upon carbachol and angiotensin II treatments respectively (Supplementary Fig. 4a,b). PM-SMC demonstrated significantly higher percentage of contractile cells than other SMC subtypes ($P = 0.036$ versus NE-SMC in carbachol; $P = 0.027$ versus NE-SMC and $P = 0.013$ versus LM-SMC in angiotensin II).

To determine whether the hPSC-derived SMCs could contribute to vessel formation *in vivo*, we implanted Matrigel plugs with our SMCs and HUVECs (ratio 1:2) subcutaneously into immunodeficient mice for two weeks. Sections were immunostained using human-specific SMTN and PECAM1 antibodies. Luminal structures comprised of HUVECs ($PECAM1^+$, green) were observed (Fig. 3d). HPSC-derived SMCs ($SMTN^+$, red) were recruited to peri-endothelial regions, reminiscent of their biological niche. There was between 30-45% SMC coverage around the endothelial vessel structures with LM-SMCs displaying lower coverage levels (31.5 ± 5.1%) than the other two groups (43.1 ± 2.6% NE-SMC and 48.9 ± 3.1 % PM-SMC). These results confirmed the *in vitro* derived SMCs were functional.

SMC subtypes recapitulate origin-specific requirement for MKL2 and unique responses to cytokines

To determine whether our system reliably generated origin-specific SMCs from hPSCs, we validated our model against reported findings from developmental studies. MKL2 is a transcriptional co-activator for serum response factor which plays a role in early embryogenesis[27]. Previous *in vivo* studies revealed the unique requirement for *Mkl2* during

SMC differentiation from neural crest but not mesoderm[28, 29]. We postulated that MKL2 was only essential for NE-SMC specification, and not for LM- or PM-SMC specification. To confirm this hypothesis, we silenced *MKL2* using small interfering RNA (siRNA) in our intermediate populations (Fig. 4a,b). We then induced SMC differentiation and found that the MKL2 siRNA-treated cells (black bars) showed a significant decrease in SMC gene expression in NE-SMC (*CNN1*, $P = 0.0006$; *MYH11*, $P = 0.015$; *SMTN*, $P = 0.0023$) compared to scrambled siRNA control (white bars) while LM-SMC and PM-SMC were unaffected (Fig. 4c). Likewise, MKL2 knockdown resulted in a significant decrease in the percentage of $MYH11^{+}/ACTA2^{+}$ NE-SMC (55.0 ± 4.8% MKL2 siRNA versus 86.7 ± 2.1% scrambled control, $P = 0.0076$, Fig. 4d), but no reduction in SMCs derived from mesoderm origins.

To ascertain that we had generated origin-specific SMC subtypes, we used cytokines known to induce unique responses in aortic SMCs of distinct origins. Angiotensin II (Ang II) promotes medial hyperplasia in the ascending aorta (neuroectoderm derivative) but not the descending aorta (mesoderm derivative)[30]. TGF-β1 also encourages greater cell proliferation in SMCs of neuroectoderm origin compared to those of mesodermal origin[31, 32]. Consistent with the previous studies, NE-SMC proliferated in response to Ang II (1 μM, red lines) and TGF-β1 (5 ng/ml, green lines) over 3 days but LM-SMC and PM-SMC did not (Fig. 4e). Serum (10%, blue lines), a potent mitogen, induced proliferation in all the SMC subtypes although to a much lesser extent in PM-SMC. Cell cycle analysis confirmed that Ang II, TGF-β1 or serum each increased the proportion of NE-SMC in S (yellow bars) and G2-M (blue bars) phases compared to vehicle control after 24 hours (Fig. 4f). LM-SMC and PM-SMC only showed higher S and G2-M populations upon serum treatment.

Only NE-SMC proliferated in response to TGF-β1 (Fig. 4e-f). This could be due to TGF-β1 enhancing cell proliferation by autocrine production of TGF-β2 and PDGFA[31, 32]. We investigated whether TGF-β1 stimulated greater auto-induction of TGF-β2 and PDGFA in SMCs of a neuroectoderm origin. Our results show that *TGFB2* ($P = 0.002$) and *PDGFA* ($P = 0.0015$) expression were significantly upregulated only in NE-SMC after 10 hours of TGF-β1 (5 ng/ml) treatment compared with vehicle control (Fig. 4g). Correspondingly, elevated TGFB2 and PDGFA protein levels were found in NE-SMC lysates after TGF-β1 treatment (Fig. 4h). Taken together, the data on requirement for MKL2 and their unique proliferative and secretory responses validate the hypothesis that our different SMC subtypes are analogous to the distinct lineage-dependent SMC populations documented *in vivo*.

SMC subtypes predict origin-dependent MMP and TIMP activation

To investigate a link between SMC developmental origins and susceptibility to vascular diseases, we treated our SMC subtypes with IL-1β (10 ng/ml), an atherogenic cytokine[33]. Rat SMCs isolated from various aortic regions (Supplementary Fig. 5) were tested in parallel. A panel of *MMP* and *TIMP* markers, known to be implicated in human atherosclerosis and aneurysm formation[34], was investigated. We discovered that, broadly, LM-SMC, NE-SMC and PM-SMC (top panel) modeled similar responses to IL-1β as the rat aortic SMCs (bottom panel) of corresponding origins – root, arch and thoracic descending (Fig. 5a). In particular, *MMP9* and *TIMP1* expression levels were differentially activated in our SMC subtypes, as were rat SMCs of distinct origins. The induction of *Mmp9* relative to control in the rat SMCs was about a 100-fold greater than that in the hPSC-derived SMCs. This could be due to species-specific variations or different degrees of SMC maturity which could reflect the differences in level of activation for certain genes. Western blot confirmed that the hPSC-derived SMCs (top panel) could predict the differential levels of MMP9 and TIMP1 proteins in the rat aortic SMCs (bottom panel) after exposure to the same stimulus

(Fig. 5b). The human SMC subtypes also predicted the differential elastin (left panel) and collagen (right panel) degradation demonstrated by the rat aortic SMCs (Fig. 5c). In summary, these results suggest that adult SMCs display heterogenous matrix remodeling responses due, in part, to their different origins. More importantly, our *in vitro* derived SMC subtypes are able to effectively model and predict the properties of their *in vivo* counterparts and consequently may have relevance in predicting origin-dependent disease responses.

Discussion

We have developed a chemically defined monolayer system to generate origin-specific vascular SMCs from hPSCs with high efficiency. The initial induction to the intermediate lineages – neuroectoderm, lateral plate mesoderm and paraxial mesoderm, is instrumental in defining our subsequent SMC subtypes. Using developmental insights on the BMP gradient along the primitive streak, we have established novel conditions for mesoderm specification. Directed differentiation towards the paraxial mesoderm has not been previously reported. Moreover, our unpatterned lateral plate mesoderm is the only non-specified tissue described to date. Other published protocols that also use BMP4, generate specific lateral plate mesoderm derivatives such as blood or cardiac lineages[19, 20, 22]. The hPSC-derived SMCs possess contractile function and participate in blood vessel formation *in vivo*. Although the SMC subtypes appear phenotypically and functionally indistinguishable, we provide evidence that they represent truly origin-specific subtypes. More specifically, we show that they recapitulate differential requirements for SMC fate commitment and unique biological responses to cytokines consistent with previous *in vivo* and *ex vivo* studies[28-32]. Uniquely, our *in vitro*-derived SMC subtypes could predict differential ECM remodeling responses of regionally distinct rat aortic SMC populations to IL-1β. Currently, findings that can discern between SMCs from the lateral plate mesoderm and paraxial mesoderm are limited. Nevertheless, we find that our PM-SMCs are less prone to serum-stimulated proliferation and ECM degradation, compared to LM-SMCs and NE-SMCs. Moreover, PM-SMCs also demonstrate greater proportions of contracting cells in response to vasoconstrictors, suggesting that PM-SMC may be relatively resistant to phenotypic modulation and retain a more differentiated phenotype than other SMC subtypes. Gene subsets uniquely upregulated in each of the SMC subtypes (Supplementary Fig. 3a) reveal previously unknown differences which may guide further studies on the functional relevance of the PM-SMC population to vascular pathology.

The diverse embryological origins of vascular SMCs are well recognized[2]. However, it remains unclear whether the site-specific presentation of some acquired vascular diseases is attributable to their intrinsic developmental origins. We have shown that origin-specific SMCs exhibit differential MMP and TIMP activation in response to IL-1β. MMP activation is associated with SMC phenotypic modulation[35], which precedes aneurysm formation in experimental models[36]. Degradation of the vessel wall connective tissues by MMPs is a major pathological remodeling process in an array of human vascular diseases[34]. We hypothesized that the differential proteolytic ability of the medial SMC subtypes could influence the weakening of the aortic wall to different extents. Consequently, regional discrepancies in vessel mechanical properties may lead to aortic dissection at the boundaries where SMCs switch origins (Fig. 6). MMPs also induce SMC migration during atheroma formation in atherosclerosis[37]. The most deleterious atherosclerotic lesions occur frequently in the coronary and carotid arteries, which arise from the lateral plate mesoderm and neuroectoderm respectively. Accordingly, our results demonstrate that LM-SMC and NE-SMC are predisposed to MMP activation more than PM-SMC. We propose that hardwired embryonic programs contribute to disease susceptibility, although recognizing that other factors such as hemodynamic forces and physical structure of the vessels also play important roles.

The described differentiation system broadly covers most of the origins of vascular SMCs. Further patterning of the intermediate lineages, for example, the lateral plate mesoderm into secondary heart field or pro-epicardial lineage, may mimic more closely the precise origins of SMCs in the aortic root and coronary artery respectively. Our protocols could potentially be extended to encompass these intermediate sub-populations in future studies. It is recognized that a small number of SMC populations may be derived from embryonic tissues beyond those that we have modeled, for example renal SMCs which are thought to originate from the metanephric mesenchyme, an intermediate mesoderm derivative, which is not modeled here. Additionally, it is likely that the hPSC-derived SMCs represent a fetal phenotype, possibly due to lack of heterotypic cell-cell interactions and *in vivo* microenvironment cues. In spite of this, our *in vitro* SMC differentiation system is the first to define conditions for generating SMCs from different embryological origins. Elucidating the molecular mechanisms underlying origin-dependent differences in SMC behavior may provide clues to understanding how SMC origins influence a variety of vascular disease patterns.

Furthermore, our ability to produce large amounts of SMC subtypes from hPSCs will be essential for far-reaching applications in vascular disease modeling and regenerative medicine. Genetic syndromes[38, 39] and hereditary influences[40-42] seem to be closely linked to SMC dysfunction in the thoracic aorta[43]. Congenital vascular diseases such as cono-truncal defects[44] or patients with CADASIL[45] feature mutations that predominantly affect neural crest-derived SMCs. Disease modeling with the appropriate origin-specific SMCs generated from patient-derived iPSCs is therefore vital for accurate assessment and therapeutic discovery. Patient matched SMCs may also be used to construct bio-engineered blood vessels for coronary and peripheral artery bypass or hemodialysis grafts. Meanwhile, for optimal outcomes in tissue or whole-organ regeneration, adequate vascularization is necessary. Hence, to maximize success in both disease modeling and regenerative medicine, it may be useful to focus on SMCs that are derived from the same embryonic lineage as in the tissue/organ affected.

Methods

HPSC culture

HESCs (lines H9 and H1 [WiCell, Madison, WI], passages 65-85) were cultured in a chemically defined medium (CDM) as previously described[46]. Human iPSCs were obtained from the Cambridge Biomedical Research Centre iPSC Core Facility (www.cambridge-brc.org.uk). Briefly, human dermal fibroblasts were isolated from excess skin of patients undergoing plastic surgery and reprogrammed as previously described[47]. Human iPSCs were grown on irradiated mouse feeders and cultured in the typical DMEM/F12 medium, containing 20% Knockout serum replacement (Gibco) and 4 ng/ml FGF-2 (R&D Systems).

HPSC differentiation

For neuroectoderm differentiation, cells were grown in CDM + SB431542 (10 μM, Tocris) + FGF2 (12 ng/ml, R&D systems) for 7 days. For early mesoderm formation, cells were initially grown in CDM+FGF2 (20 ng/ml, R&D Systems) + LY294002 (10 μM, Sigma) + BMP4 (10 ng/ml, R&D Systems) for 36 hours. Further specification into lateral plate mesoderm required CDM+FGF2 (20 ng/ml, R&D Systems) + BMP4 (50 ng/ml, R&D Systems) for another 3.5 days; whereas paraxial mesoderm required CDM+FGF2 (20 ng/ml, R&D Systems) + LY294002 (10 μM, Sigma). Upon obtaining the intermediate populations, cells were trypsinised and cultured in SMC differentiation medium CDM+PDGF-BB (10 ng/ml, PeproTech) + TGF-β1 (2 ng/ml, PeproTech) for at least 12 days. Derived SMCs were

maintained in CDM deprived of growth factors for at least 24 hours before subsequent experiments.

Quantitative real-time polymerase chain reaction (QRTPCR)

Total RNA was extracted with RNeasy Mini kit according to the manufacturer's instructions (QIAGEN). cDNA was prepared using Maxima First Strand cDNA Synthesis Kit (Fermentas). QRTPCR mixtures were prepared with SYBR Green PCR Master Mix (Applied Biosystems). QRTPCR reactions were performed in technical duplicates with the 7500 Fast Real-time PCR System (Applied Biosystems), using the Quantitation – comparative C_T settings. Obtained values were normalized to Porphobilinogen Deaminase (PBGD). Primer sequences are listed in Supplementary Table 2.

Immunofluorescence and flow cytometry

For immunofluorescence, adherent cells were fixed and permabilized. After blocking with 3% BSA, primary antibody was incubated at 4 °C overnight. Secondary goat anti-mouse Alexa Fluor 568 and goat anti-rabbit Alexa Fluor 488 antibodies (Invitrogen Molecular Probes) were used. Finally, nuclei were stained with DAPI. Images were acquired by Zeiss Axiovert 200M microscope. For flow cytometry, harvested cells were fixed using the Cytofix/Cytoperm Fixation/Permeabilization kit (BD Biosceinces) and stained according to the kit manual. Mouse IgG isotype controls (BD PharMingen, 555749, R&D Systems, IC002C) and non-expressing cell controls (H9 hESCs and HUVECs) were used. Primary antibodies used for this study are listed in Supplementary Table 3.

Western blot

30 μg of total protein was resolved with SDS-PAGE and transferred to nitrocellulose membranes. The membrane was probed with primary antibodies (Supplementary Table 3) and secondary anti-rabbit-HRP (Sigma) and anti-mouse-HRP (Sigma) antibodies. Detection was performed using the ECL system (GE Healthcare).

Microarray analysis

The Illumina HumanHT-12 v4 BeadArray (http://www.illumina.com/) was used to obtain global gene expression of hESC and SMC samples. Acquired data was processed with *R* statistical programming environment (http://www.r-project.org). Raw and processed data are available from the ArrayExpress microarray data repository (http://www.ebi.ac.uk/microarray-as/ae/) under accession numbers E-MTAB-781 (SMC) and E-MTAB-464 (hESC). Heatmaps of relative gene expression were generated with the Heatmap Builder software[48] (downloaded courtesy of the Ashley Lab, Stanford). The statistical over-representation of functional gene categories ($p < 0.01$) among genes deemed differentially expressed between sample group profiles was assessed using the functional annotation clustering from the DAVID bioinformatics resource[49]. Refer to Supplementary Methods for a detailed description of microarray methods.

Cell migration assay

Scratch assay was performed as previously described[50].

Contraction study

SMCs were preloaded with the calcium-sensitive fluorophore, Fluo-4 AM (2.5 μM; Molecular Probes) at 37°C for an hour. Contraction was induced by treating the cells with carbachol (100 μM, Sigma). Intracellular calcium flux was measured using the FL1 channel of CyAn ADP flow cytometer (Beckman Coulter). Contraction videos of SMCs were

Europe PMC Funders Author Manuscripts

acquired by a time-lapse microscope (Olympus IX700) during 10 minutes of carbachol treatment. Change of cell surface area was assessed by ImageJ software.

Matrigel plug implantation

In vivo studies were compliant with the UK Home Office: Animals In Scientific Procedures guidelines and approved by the University of Cambridge. Derived SMCs and HUVECs (ratio 1:2) were resuspended in ice cold matrigel basement membrane matrix (BD Biosciences) at a final cell concentration of 10^6 cells/ml. 750 μl of cell suspension was injected subcutaneously into Rag2-null immunodeficient male mice. After 2 weeks, the animals were sacrificed and the matrigel plugs were excised to be paraffin embedded. The sections were then immunostained and imaged with a confocal microscope (Zeiss, LSM700).

Short interfering RNA (siRNA) gene silencing

Transient knockdown of MKL2 was carried out with ON-TARGETplus SMARTpool siRNA by DharmaFECT transfection reagent (Thermo Scientific Dharmacon). 10 nM of siRNA was used for transfection according to the manufacturer's instructions. Messenger RNA and protein analyses were performed at 24 hours and 48 hours post-transfection respectively.

Proliferation assays

For cell proliferation assay, hESC-derived SMCs were seeded 6,000 cells/well into 96-well plates. Following incubation overnight, TGF-β1 (5 ng/ml, PeproTech), angiotensin II (10 μM, Sigma) or 10% FBS (Sigma) was added. Cell viability was measured as a function of the metabolic activity using tetrazolium salt, MTT (Sigma). At every timepoint, MTT (0.5 mg/ml) was incubated with the cells at 37°C for 2 hours and then solubilized using DMSO (Sigma) at 37°C for 15 min. Absorbance was measured at 550 nm using the Wallac Envision 2104 multilabel reader (PerkinElmer). For cell cycle analysis, hESC-derived SMCs were harvested and the cell suspension was fixed by ice cold 70% ethanol for 30 minutes at 4°C. To ensure that only DNA is stained, cells were treated with 100 μg/ml of ribonuclease. Finally, cells were stained with 50 μg/ml of propidium iodide in the dark at room temperature for 30 minutes. Cell fluorescence was measured by a flow cytometer (Beckman Coulter CyAn ADP) and cell cycle analysis was performed using FlowJo software.

Rat primary SMC culture

Rats were euthanized using carbon dioxide and different aortic regions were surgically dissected. Aortic segments were incubated with 12.5 ml of enzyme solution composing of 1 mg/ml collagenase II (Worthington), 1 mg/ml soybean trypsin inhibitor (Worthington), 9.3 units activity elastase (Worthington), 125 μl pen-strep and 12.5 ml HBSS (Gibco) for 20 minutes at 37°C. Adventitia was removed and aortic segments were rinsed to remove intimal cells. Remaining medial segments were snipped into 0.5-1 mm pieces and enzyme treated again for 1 hour with occasional agitation. Dissociated SMCs were cultured in DMEM supplemented with 10% FBS, 100 U/mL of penicillin and 100 mg/mL of streptomycin. Rat SMCs were serum-starved for at least 24 hours before experimentation. All experiments were performed with cells during passages 2–4.

Proteolytic assays

96-well plates were coated with either 0.1 mg/ml of elastin or collagen type I, of which both were FITC conjugated (AnaSpec). HESC-derived SMCs or rat SMCs were then seeded 6,000 cells/well. Following incubation overnight, 10 ng/ml of IL-1β (PeproTech) was added in serum-free media. Activity of secreted proteases was assessed by the increase of

Europe PMC Funders Author Manuscripts

fluorescence measured at excitation/emission = 490 nm/ 520 nm using the Wallac Envision 2104 multilabel reader (PerkinElmer). To take into account any differential cell proliferation due to IL-1β, the fluorescence readout was normalized against the corresponding cell number/well.

Statistics

Results are presented as mean ± s.e.m. of 3 independent experiments unless otherwise stated. Statistical *P* values were calculated by Student's *t*-test unless otherwise stated. Significant differences are indicated as $*P < 0.05$; $^{+}P < 0.01$; $\wedge P < 0.001$.

Supplementary Material

Refer to Web version on PubMed Central for supplementary material.

Acknowledgments

The authors thank Dr L. Vallier and Dr S.T. Rashid for supplying us the wild-type human iPSCs; Dr K. Jensen for the human fetal gut RNA; Ms N. Figg and Mr M. Ackers-Johnson for help rendered in matrigel sectioning and the harvesting of rat aortic SMCs respectively. We also thank Mr T. Faial and Mr D. Ortmann for validation of the mesoderm protocols. This work was supported by a Wellcome Trust Intermediate Clinical Fellowship for S Sinha and the Cambridge NIHR Comprehensive Biomedical Research Centre. C. Cheung was sponsored by a National Science Scholarship (PhD) from Agency for Science, Technology and Research (Singapore). R.A. Pedersen, and M. Trotter were supported by a MRC centre grant and A.S. Bernardo was supported by a Leukemia and Lymphoma Society grant.

References

1. Carmeliet P. Mechanisms of angiogenesis and arteriogenesis. Nature medicine. 2000; 6:389–395.
2. Majesky MW. Developmental basis of vascular smooth muscle diversity. Arteriosclerosis, thrombosis, and vascular biology. 2007; 27:1248–1258.
3. Waldo KL, et al. Secondary heart field contributes myocardium and smooth muscle to the arterial pole of the developing heart. Developmental biology. 2005; 281:78–90. [PubMed: 15848390]
4. Jiang X, Rowitch DH, Soriano P, McMahon AP, Sucov HM. Fate of the mammalian cardiac neural crest. Development. 2000; 127:1607–1616. [PubMed: 10725237]
5. Wasteson P, et al. Developmental origin of smooth muscle cells in the descending aorta in mice. Development. 2008; 135:1823–1832. [PubMed: 18417617]
6. Mikawa T, Gourdie RG. Pericardial mesoderm generates a population of coronary smooth muscle cells migrating into the heart along with ingrowth of the epicardial organ. Developmental biology. 1996; 174:221–232. [PubMed: 8631495]
7. Etchevers HC, Vincent C, Le Douarin NM, Couly GF. The cephalic neural crest provides pericytes and smooth muscle cells to all blood vessels of the face and forebrain. Development. 2001; 128:1059–1068. [PubMed: 11245571]
8. Peeters, M.P. Vrancken; Gittenberger-de Groot, AC.; Mentink, MM.; Poelmann, RE. Smooth muscle cells and fibroblasts of the coronary arteries derive from epithelial-mesenchymal transformation of the epicardium. Anatomy and embryology. 1999; 199:367–378. [PubMed: 10195310]
9. Pouget C, Pottin K, Jaffredo T. Sclerotomal origin of vascular smooth muscle cells and pericytes in the embryo. Developmental biology. 2008; 315:437–447. [PubMed: 18255054]
10. Armulik A, Genove G, Betsholtz C. Pericytes: developmental, physiological, and pathological perspectives, problems, and promises. Developmental cell. 2011; 21:193–215. [PubMed: 21839917]
11. Haimovici H, Maier N. Fate of Aortic Homografts in Canine Atherosclerosis. 3. Study of Fresh Abdominal and Thoracic Aortic Implants into Thoracic Aorta: Role of Tissue Susceptibility in Atherogenesis. Arch Surg. 1964; 89:961–969. [PubMed: 14208469]

12. DeBakey ME, Lawrie GM, Glaeser DH. Patterns of atherosclerosis and their surgical significance. Annals of surgery. 1985; 201:115–131. [PubMed: 3155934]
13. Leroux-Berger M, et al. Pathologic calcification of adult vascular smooth muscle cells differs on their crest or mesodermal embryonic origin. Journal of bone and mineral research : the official journal of the American Society for Bone and Mineral Research. 2011; 26:1543–1553. [PubMed: 21425330]
14. Ruddy JM, Jones JA, Spinale FG, Ikonomidis JS. Regional heterogeneity within the aorta: relevance to aneurysm disease. The Journal of thoracic and cardiovascular surgery. 2008; 136:1123–1130. [PubMed: 19026791]
15. Cheung C, Sinha S. Human embryonic stem cell-derived vascular smooth muscle cells in therapeutic neovascularisation. Journal of molecular and cellular cardiology. 2011; 51:651–664. [PubMed: 21816157]
16. Vallier L, et al. Early cell fate decisions of human embryonic stem cells and mouse epiblast stem cells are controlled by the same signalling pathways. PloS one. 2009; 4:e6082. [PubMed: 19564924]
17. Bernardo AS, et al. BRACHYURY and CDX2 mediate BMP-induced differentiation of human and mouse pluripotent stem cells into embryonic and extraembryonic lineages. Cell stem cell. 2011; 9:144–155. [PubMed: 21816365]
18. Dosch R, Gawantka V, Delius H, Blumenstock C, Niehrs C. Bmp-4 acts as a morphogen in dorsoventral mesoderm patterning in Xenopus. Development. 1997; 124:2325–2334. [PubMed: 9199359]
19. Schneider MD, Gaussin V, Lyons KM. Tempting fate: BMP signals for cardiac morphogenesis. Cytokine & growth factor reviews. 2003; 14:1–4. [PubMed: 12485614]
20. Goldman DC, et al. BMP4 regulates the hematopoietic stem cell niche. Blood. 2009; 114:4393–4401. [PubMed: 19759357]
21. Zhang P, et al. Short-term BMP-4 treatment initiates mesoderm induction in human embryonic stem cells. Blood. 2008; 111:1933–1941. [PubMed: 18042803]
22. Yang L, et al. Human cardiovascular progenitor cells develop from a KDR+ embryonic-stem-cell-derived population. Nature. 2008; 453:524–528. [PubMed: 18432194]
23. McLean AB, et al. Activin a efficiently specifies definitive endoderm from human embryonic stem cells only when phosphatidylinositol 3-kinase signaling is suppressed. Stem Cells. 2007; 25:29–38. [PubMed: 17204604]
24. Jain RK. Molecular regulation of vessel maturation. Nature medicine. 2003; 9:685–693.
25. Kramer J, Quensel C, Meding J, Cardoso MC, Leonhardt H. Identification and characterization of novel smoothelin isoforms in vascular smooth muscle. Journal of vascular research. 2001; 38:120–132. [PubMed: 11316948]
26. Huang X, Saint-Jeannet JP. Induction of the neural crest and the opportunities of life on the edge. Developmental biology. 2004; 275:1–11. [PubMed: 15464568]
27. Wang DZ, et al. Potentiation of serum response factor activity by a family of myocardin-related transcription factors. Proceedings of the National Academy of Sciences of the United States of America. 2002; 99:14855–14860. [PubMed: 12397177]
28. Li J, et al. Myocardin-related transcription factor B is required in cardiac neural crest for smooth muscle differentiation and cardiovascular development. Proceedings of the National Academy of Sciences of the United States of America. 2005; 102:8916–8921. [PubMed: 15951419]
29. Oh J, Richardson JA, Olson EN. Requirement of myocardin-related transcription factor-B for remodeling of branchial arch arteries and smooth muscle differentiation. Proceedings of the National Academy of Sciences of the United States of America. 2005; 102:15122–15127. [PubMed: 16204380]
30. Owens AP 3rd, et al. Angiotensin II induces a region-specific hyperplasia of the ascending aorta through regulation of inhibitor of differentiation 3. Circulation research. 2010; 106:611–619. [PubMed: 20019328]
31. Topouzis S, Majesky MW. Smooth muscle lineage diversity in the chick embryo. Two types of aortic smooth muscle cell differ in growth and receptor-mediated transcriptional responses to transforming growth factor-beta. Developmental biology. 1996; 178:430–445.

32. Gadson PF Jr. et al. Differential response of mesoderm- and neural crest-derived smooth muscle to TGF-beta1: regulation of c-myb and alpha1 (I) procollagen genes. Experimental cell research. 1997; 230:169–180. [PubMed: 9024776]
33. Isoda K, et al. Deficiency of interleukin-1 receptor antagonist promotes neointimal formation after injury. Circulation. 2003; 108:516–518. [PubMed: 12874179]
34. Galis ZS, Khatri JJ. Matrix metalloproteinases in vascular remodeling and atherogenesis: the good, the bad, and the ugly. Circulation research. 2002; 90:251–262. [PubMed: 11861412]
35. Owens GK, Kumar MS, Wamhoff BR. Molecular regulation of vascular smooth muscle cell differentiation in development and disease. Physiological reviews. 2004; 84:767–801. [PubMed: 15269336]
36. Ailawadi G, et al. Smooth muscle phenotypic modulation is an early event in aortic aneurysms. The Journal of thoracic and cardiovascular surgery. 2009; 138:1392–1399. [PubMed: 19931668]
37. Libby P, Ridker PM, Hansson GK. Progress and challenges in translating the biology of atherosclerosis. Nature. 2011; 473:317–325. [PubMed: 21593864]
38. Milewicz DM, Dietz HC, Miller DC. Treatment of aortic disease in patients with Marfan syndrome. Circulation. 2005; 111:e150–157. [PubMed: 15781745]
39. Loeys BL, et al. A syndrome of altered cardiovascular, craniofacial, neurocognitive and skeletal development caused by mutations in TGFBR1 or TGFBR2. Nature genetics. 2005; 37:275–281. [PubMed: 15731757]
40. Zhu L, et al. Mutations in myosin heavy chain 11 cause a syndrome associating thoracic aortic aneurysm/aortic dissection and patent ductus arteriosus. Nature genetics. 2006; 38:343–349. [PubMed: 16444274]
41. Guo DC, et al. Mutations in smooth muscle alpha-actin (ACTA2) lead to thoracic aortic aneurysms and dissections. Nature genetics. 2007; 39:1488–1493. [PubMed: 17994018]
42. van de Laar IM, et al. Mutations in SMAD3 cause a syndromic form of aortic aneurysms and dissections with early-onset osteoarthritis. Nature genetics. 2011; 43:121–126. [PubMed: 21217753]
43. Lindsay ME, Dietz HC. Lessons on the pathogenesis of aneurysm from heritable conditions. Nature. 2011; 473:308–316. [PubMed: 21593863]
44. Gittenberger-de Groot AC, Bartelings MM, Deruiter MC, Poelmann RE. Basics of cardiac development for the understanding of congenital heart malformations. Pediatric research. 2005; 57:169–176. [PubMed: 15611355]
45. Kalimo H, Ruchoux MM, Viitanen M, Kalaria RN. CADASIL: a common form of hereditary arteriopathy causing brain infarcts and dementia. Brain Pathol. 2002; 12:371–384. [PubMed: 12146805]
46. Brons IG, et al. Derivation of pluripotent epiblast stem cells from mammalian embryos. Nature. 2007; 448:191–195. [PubMed: 17597762]
47. Vallier L, et al. Signaling pathways controlling pluripotency and early cell fate decisions of human induced pluripotent stem cells. Stem Cells. 2009; 27:2655–2666. [PubMed: 19688839]
48. King JY, et al. Pathway analysis of coronary atherosclerosis. Physiological genomics. 2005; 23:103–118. [PubMed: 15942018]
49. Dennis G Jr. et al. DAVID: Database for Annotation, Visualization, and Integrated Discovery. Genome biology. 2003; 4:P3. [PubMed: 12734009]
50. Liang CC, Park AY, Guan JL. In vitro scratch assay: a convenient and inexpensive method for analysis of cell migration in vitro. Nature protocols. 2007; 2:329–333.

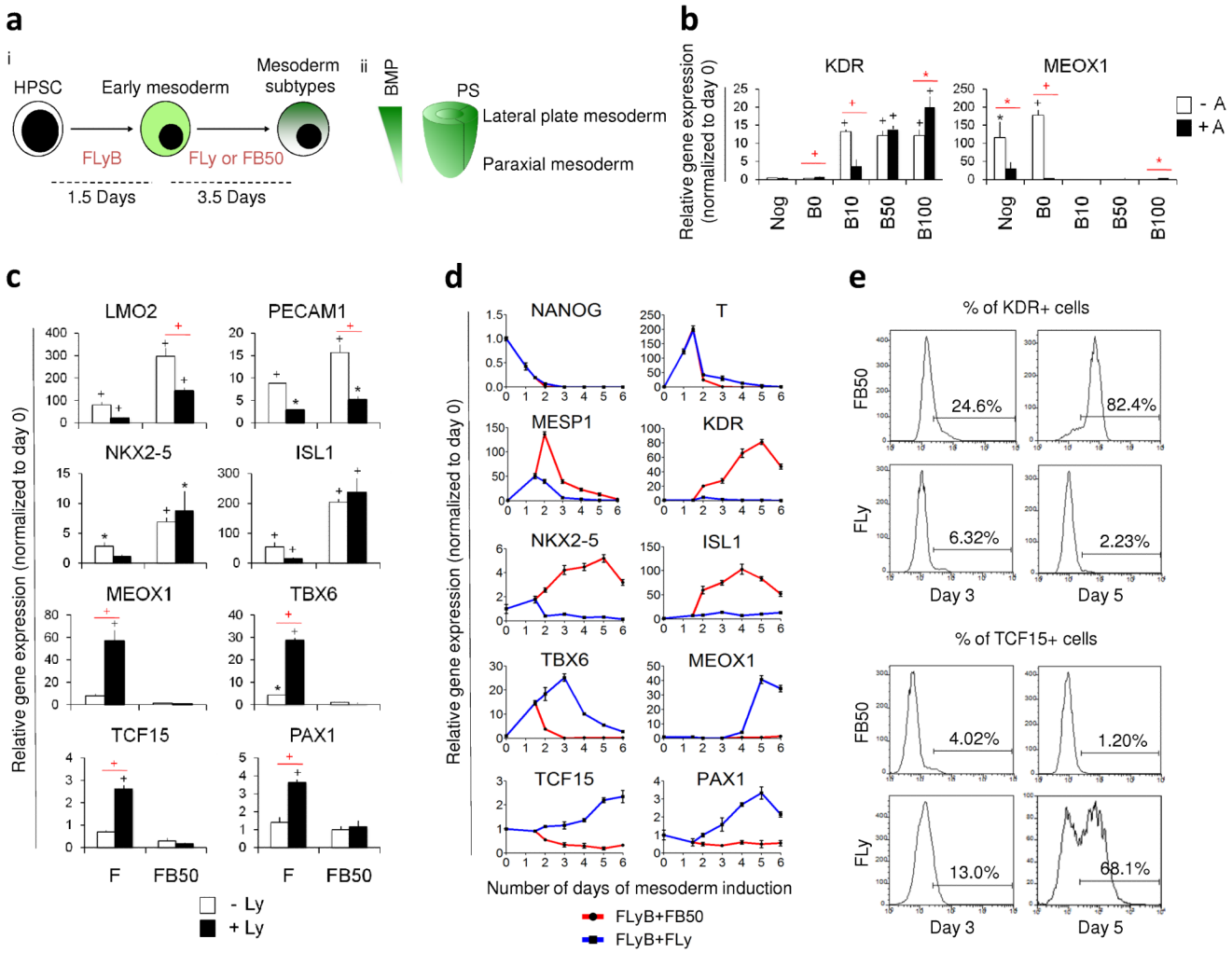

Figure 1.

Induction of mesoderm subtypes from hPSCs. (**a**) (i) HPSCs were initially differentiated to early mesoderm using FGF2, LY294002 and BMP4 (depicted as FLyB) for 36 hours. Mesoderm subtype specification required another 3.5 days of FGF2+LY294002 (FLy) or FGF2+BMP4 (FB) for paraxial or lateral plate induction. (ii) BMP concentration gradient exists along the primitive streak (PS). On the basis of fate map studies, mesoderm subtypes emerge along the gradient on the embryo cylinder. (**b**) *KDR* and *MEOX1* expression levels of hESCs differentiated for 36 hours in FLyB, followed by 3.5 days in FGF2+LY294002 with Noggin (Nog), BMP4 (B) and/or Activin (A) were determined by QRTPCR. BMP4 concentrations ranged from 0 ng/ml (B0) to 100 ng/ml (B100). (**c**) Lateral plate and paraxial

Europe PMC Funders Author Manuscripts

mesoderm marker expression levels in hESCs differentiated for 36 hours in FLyB and then 3.5 additional days in FGF2 (F) or FGF2+BMP4 (FB50, where BMP4 is 50 ng/ml), with (black bars) or without (white bars) LY294002 (Ly) determined by QRTPCR. (**d**) Temporal QRTPCR to analyze mesoderm specification. Following a common 36-hour treatment of FLyB, lateral and paraxial mesoderms were specified using FB50 (red line) and FLy (blue line) respectively. (**e**) Percentage of KDR^+ and $TCF15^+$ cells at days 3 and 5 determined by flow cytometry. (**f**) At day 5, FB50- and FLy-treated populations were immunostained for mesoderm subtype-specific markers. Scale bars, 100 μm. Data represent means ± s.e.m. (n = 3). Significant differences compared to day 0 population are indicated in black, while that between two groups are indicated in red (*$P < 0.05$; $^+P < 0.01$; ^$P < 0.001$).

Europe PMC Funders Author Manuscripts

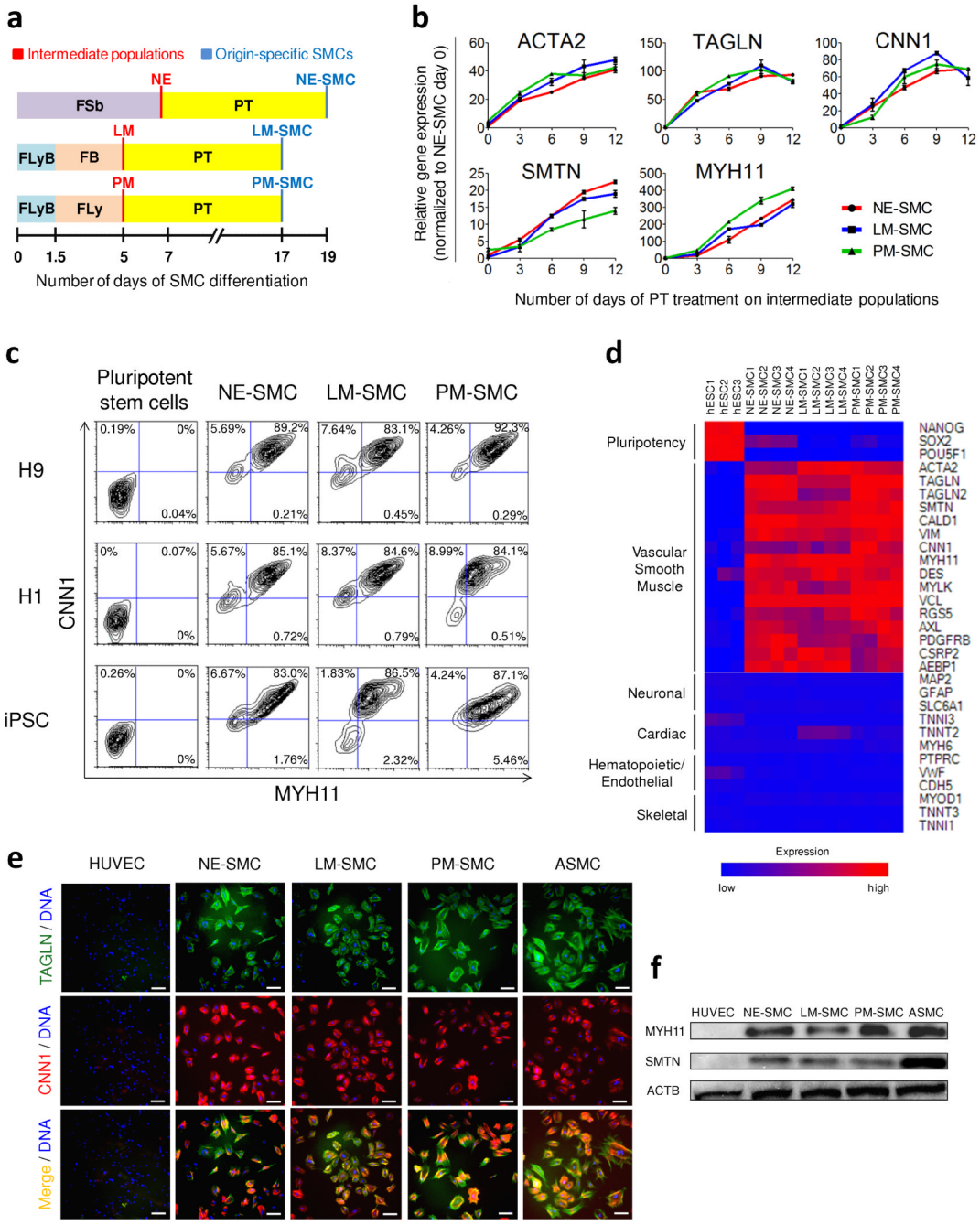

Figure 2.

Efficient differentiation of intermediate lineages into vascular SMCs. (**a**) A schematic which outlines the conditions for deriving origin-specific SMCs from hPSCs. FLyB+FB and FLyB +FLy have been described in Figure 1 to generate the lateral plate mesoderm (LM) and paraxial mesoderm (PM) respectively. HPSCs were treated with FGF2+SB431542 (FSb) for 7 days to induce neuroectoderm (NE) differentiation. For further differentiation into vascular SMCs, each intermediate population was subjected to PDGF-BB+TGF-β1 (PT) for 12 additional days. The SMC subtypes, namely the neuroectoderm-derived SMC, lateral mesoderm-derived SMC, paraxial mesoderm-derived SMC are abbreviated as NE-SMC, LM-SMC and PM-SMC respectively. (**b**) QRTPCR demonstrated increasing expression of

Europe PMC Funders Author Manuscripts

SMC markers during the 12 days of PT treatment on the three intermediate populations. Data represent means ± s.e.m. (n = 3). (**c**) Flow cytometric analysis demonstrated that the SMC differentiation protocols were highly efficient and reproducible in three hPSC lines with 83-92% of the resulting populations double positive for MYH11 and CNN1. (**d**) Microarray gene expression heat map of control hESCs versus SMC subtypes obtained after 12 days of PT treatment. Red (upregulation) and blue (downregulation) depict differential gene expression from the mean across all samples. (**e**) The majority of our SMC subtypes immunostained positively for CNN1 (red) and TAGLN (green). Human umbilical vein endothelial cell (HUVEC) was used as a negative control, while ASMC was used as a positive control. Scale bars, 100 μm. (**f**) Western blot confirmed the presence of the mature SMC proteins, MYH11 and SMTN, in the hPSC-derived SMCs and ASMC but not HUVEC.

Europe PMC Funders Author Manuscripts

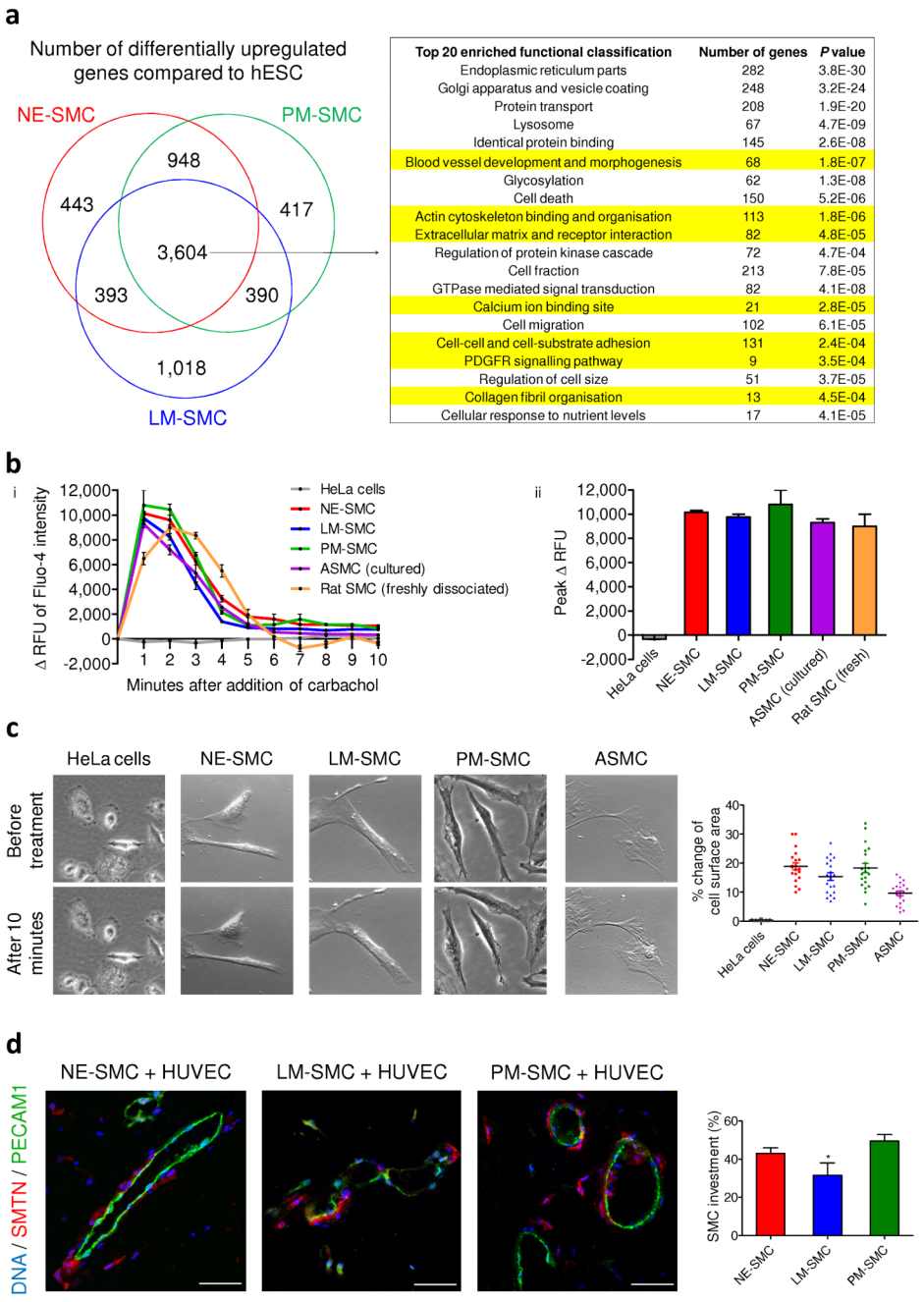

Top 20 enriched functional classification	Number of genes	*P* value
Endoplasmic reticulum parts	282	3.8E-30
Golgi apparatus and vesicle coating	248	3.2E-24
Protein transport	208	1.9E-20
Lysosome	67	4.7E-09
Identical protein binding	145	2.6E-08
Blood vessel development and morphogenesis	68	1.8E-07
Glycosylation	62	1.3E-08
Cell death	150	5.2E-06
Actin cytoskeleton binding and organisation	113	1.8E-06
Extracellular matrix and receptor interaction	82	4.8E-05
Regulation of protein kinase cascade	72	4.7E-04
Cell fraction	213	7.8E-05
GTPase mediated signal transduction	82	4.1E-08
Calcium ion binding site	21	2.8E-05
Cell migration	102	6.1E-05
Cell-cell and cell-substrate adhesion	131	2.4E-04
PDGFR signalling pathway	9	3.5E-04
Regulation of cell size	51	3.7E-05
Collagen fibril organisation	13	4.5E-04
Cellular response to nutrient levels	17	4.1E-05

Figure 3.

Functional characterization of hPSC-derived SMCs. (**a**) Based on global gene expression profiles, the Venn diagram represent subsets of genes that were differentially upregulated in the SMC subtypes compared to hESC (FDR 0.1%). The commonly upregulated 3,604 genes were analyzed using the functional annotation clustering from DAVID bioinformatics resources. Among the top 20 highly enriched groups, functional characteristics pertaining to vascular SMCs are highlighted in yellow. (**b**) (i) Change in the relative fluorescence unit (Δ RFU) of Fluo-4 loaded cells was monitored by flow cytometry over 10 minutes after the addition of carbachol, an inducer of contraction. (ii) Peak Δ RFU of Fluo-4 intensity in

response to carbachol in the derived SMCs and the SMC controls ($n = 3$). (**c**) HPSC-derived SMCs and ASMC displayed contractile ability in response to carbachol treatment. There was a 10-20% change of surface area in contracting cells of all SMCs except HeLa cells ($n = 20$). (**d**) Matrigel plugs were harvested 2 weeks after the subcutaneous implantation of hPSC-derived SMCs and HUVECs (1:2). Histological sections were then double immunostained with human-specific SMTN and PECAM1 antibodies. SMC investment was quantified based on the relative length of endothelial luminal structures (green) that had SMC coverage (red) in 10 different optical fields. Statistical test was performed by ANOVA (*$P < 0.05$). Scale bars, 50 μm.

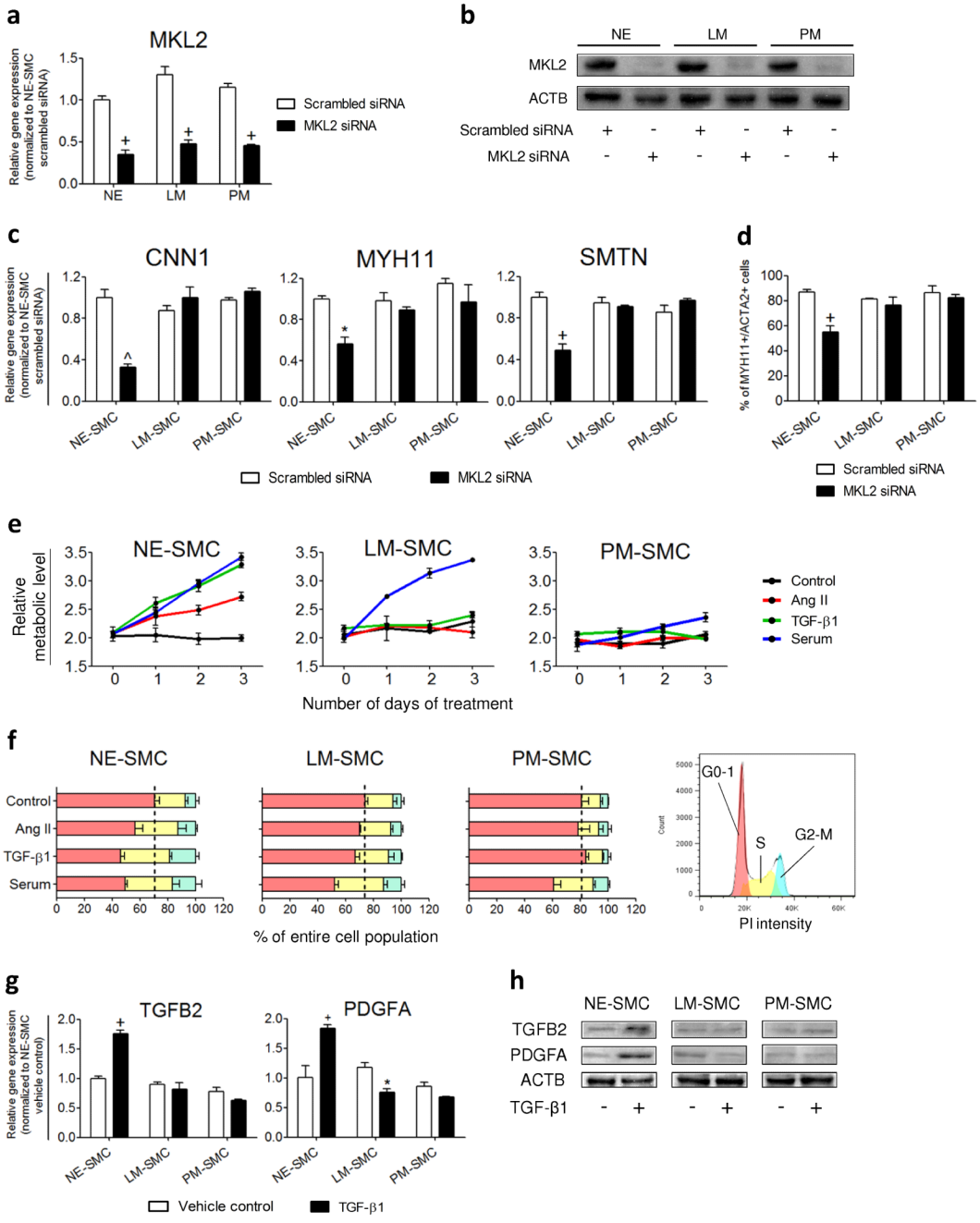

Figure 4.

MKL2 knockdown and cytokine treatments validate the origin-specific characteristics of hPSC-derived SMC subtypes. (**a**) 60-65% knockdown of the *MKL2* expression levels in the intermediate populations (NE, LM and PM) by MKL2 siRNA was verified by QRTPCR. (**b**) Western blot analysis confirmed the effects of MKL2 siRNA knockdown on the protein levels compared to scrambled siRNA controls. (**c**) SMC gene expression levels after SMC differentiation of the siRNA-treated intermediate populations were determined by QRTPCR. (**d**) Percentage of $MYH11^{+}/ACTA2^{+}$ SMCs obtained from the siRNA-treated intermediate populations was determined by flow cytometry. (**e**) Proliferation responses of the SMC

subtypes were monitored by MTT assay every 24 hours over 3 days of treatment with the cytokines indicated. (**f**) Cell cycle analysis of the SMC subtypes after 24 hours of cytokine treatments. The percentage of cells in different phases of cell cycle was quantified by the areas under the red peak (G0-G1), the area shaded yellow (S) and under the blue peak (G2-M) (legend on the right). Black dotted lines divide the growth arrested cells in G0-G1 from the proliferating cells in S and G2-M of the control groups. (**g**) Gene expression levels in control and TGF-β1-treated SMCs were determined by QRTPCR after 10 hours of treatment. (**h**) Western blot analysis was performed to confirm the distinct secretory responses exhibited by TGF-β1-treated SMC subtypes. Data represent means ± s.e.m. (n = 3). Significant differences compared to the scrambled siRNA or vehicle controls are indicated (*$P < 0.05$; $^{+}P < 0.01$, ^$P < 0.001$).

Europe PMC Funders Author Manuscripts

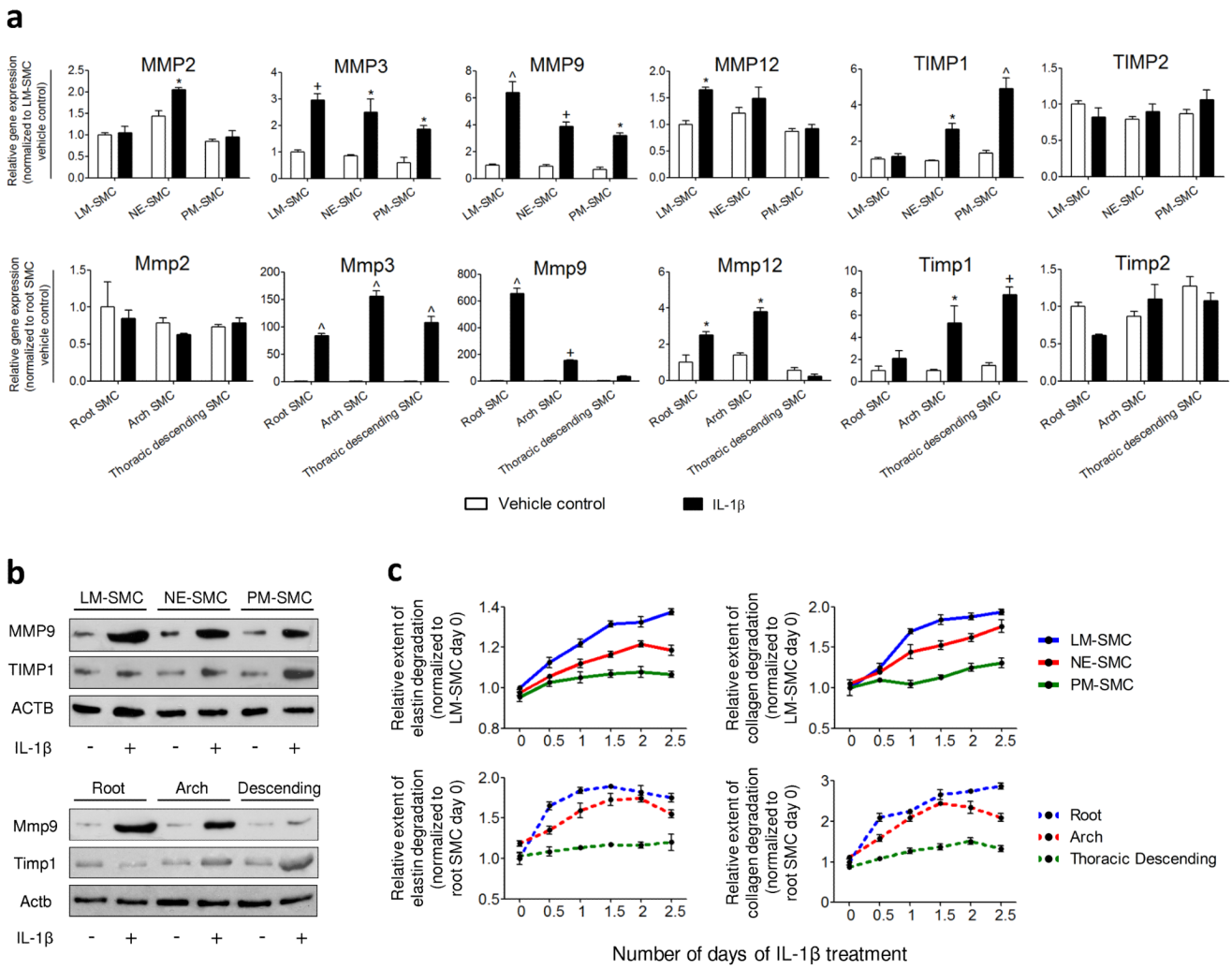

Figure 5.

HPSC-derived SMC subtypes predict MMP and TIMP expression and activity in rat aortic SMCs of corresponding origins. (**a**) Gene expression levels of MMPs and TIMPs in control (white bars) and IL-1β-treated SMCs (black bars) were determined by QRTPCR after 6 hours of treatment. Differential activation of *MMP9* and *TIMP1* expression was observed in both the hPSC-derived SMCs (top panel) and rat aortic SMCs (bottom panel). (**b**) Western blot analysis confirmed the differential amounts of MMP9 and TIMP1 proteins in the IL-1β-treated SMCs of unique origins. (**c**) Proteolytic abilities of the SMCs were assessed by elastase and collagenase assays over 2.5 days. The origin-specific SMCs (top panel) replicated similar trends of elastin and collagen degradation as the rat aortic SMCs (bottom panel) in response to IL-1β. Data represent means ± s.e.m. ($n = 3$). Significant differences compared to the vehicle controls (*$P < 0.05$; $^{+}P < 0.01$; ^$P < 0.001$).

Europe PMC Funders Author Manuscripts

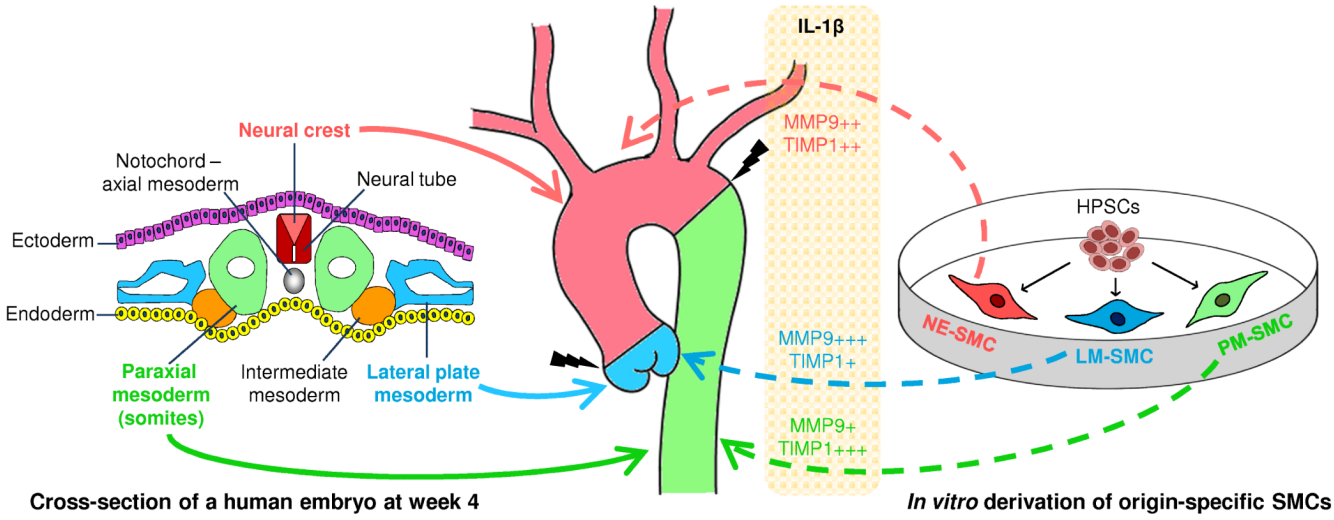

Figure 6.

The different embryological origins of aortic SMCs may contribute to the site of aortic dissection. Aortic SMCs originate from three distinct developmental lineages. The aortic root is derived from secondary heart field, a lateral plate mesoderm derivative (blue solid arrow), while the ascending aorta and arch are neural crest derived (red solid arrow). The descending aortic SMCs originate from paraxial/somitic mesoderm (green solid arrow). In this study, our *in vitro* hPSC-derived SMC subtypes predicted the differential MMP and TIMP activation in aortic SMCs of corresponding origins (dotted arrows) in response to an inflammatory mediator, IL-1β. We propose that the origin-specific SMCs display differential proteolytic ability in disease settings, which may result in differential loss of the structural integrity in different regions along the aortic wall. Such a difference in mechanical properties may predispose the sites of aortic dissection to occur preferentially at the boundaries between different SMC lineages (indicated by black jagged bolts).

Europe PMC Funders Author Manuscripts